ADVANCING EARTH AND SPACE SCIENCES

JGR Space Physics

RESEARCH ARTICLE
10.1029/2024JA033592

Special Collection:
Recent Discoveries in Substorm Research

Separating DP1 and DP2 Current Pattern Contributions to Substorm-Like Intensifications in SML

C. J. Lao[1], C. Forsyth[1], M. P. Freeman[1,2], and J. W. Gjerloev[3]

[1]UCL, Mullard Space Science Laboratory, Dorking, UK, [2]British Antarctic Survey, Cambridge, UK, [3]Johns Hopkins University Applied Physics Laboratory, Laurel, MD, USA

Key Points:

- The events in the Substorm Onsets and PHases from Indices of the Electrojets substorm phase list (Forsyth et al., 2015, https://doi.org/10.1002/2015ja021343) can be separated into DP1 or DP2 current system contributions
- There is a notable contribution (59%) to SML bays by enhancements of the DP2 equivalent current system
- For AL/SML based substorm lists more information is required to filter out false positive substorm events

Supporting Information:

Supporting Information may be found in the online version of this article.

Correspondence to:

C. J. Lao,
christian.lao.21@ucl.ac.uk

Citation:

Lao, C. J., Forsyth, C., Freeman, M. P., & Gjerloev, J. W. (2025). Separating DP1 and DP2 current pattern contributions to substorm-like intensifications in SML. *Journal of Geophysical Research: Space Physics*, *130*, e2024JA033592. https://doi.org/10.1029/2024JA033592

Received 27 NOV 2024
Accepted 20 APR 2025

Abstract Substorms have been identified from negative bays in the AL/SML index, which traces the minimum northward ground magnetic deflection at auroral latitudes, produced by enhancements of the westward electrojet. For substorms, negative bays are caused by the closure of the Substorm Current Wedge through the ionosphere, typically localized to the nightside and centered around 23-00 magnetic local time (MLT). In this case, the equivalent current pattern that causes the magnetic deflections is given the name Disturbance Polar (DP) 1. However, negative bays may also form when the westward electrojet is enhanced by increased convection, driving Pedersen and Hall currents in the auroral zone. Convection enhancements also strengthen the eastward electrojet, monitored by AU/SMU index. In this case, the equivalent current pattern that produces the magnetic deflections is called DP2. Unlike other substorm identification methods, the Substorm Onsets and PHases from Indices of the Electrojets technique by Forsyth et al. (2015), https://doi.org/10.1002/2015ja021343 attempts to distinguish between the DP1 and DP2 enhancements that cause substorm-like SML bays. Despite this, we find evidence that between 1997 and 2019 up to 59% of the 30,329 events originally identified as substorms come from enhancements of DP2 on top of the 2,627 convection enhancement events already identified. We explore ways to improve substorm identification using auroral indices to fully separate the DP1 and DP2 bays but conclude that there is insufficient information in the auroral indices to achieve this. In reality, any "substorm" list is a list of magnetic enhancements, auroral enhancements, etc., which may or may not correspond to substorm activity and should be treated that way.

1. Introduction

The substorm is a magnetospheric process during which magnetic flux is accumulated and then suddenly released in the magnetotail, typically described as a loading-unloading process. The classical description of the substorm includes 3 phases: growth, expansion, and recovery (Akasofu, 1964; McPherron, 1970). The growth phase is initiated by a southward turning of the interplanetary magnetic field and enhanced dayside reconnection (McPherron, 1970). This acts to add to the stored magnetic flux in the tail lobes, resulting in a thinning of the plasma sheet and enhancing the cross-tail current. The onset of the substorm expansion phase occurs as the localized brightening of an equatorward arc, followed by its spread poleward and azimuthally (Akasofu, 1964; Kalmoni et al., 2017). At a similar time, there is the formation of the substorm current wedge (SCW) in the inner magnetotail, where the intensified tail current is disrupted, and a pair of field-aligned currents couples the magnetotail with the ionosphere (Kepko et al., 2015; McPherron et al., 1973). This closure in the ionosphere is observed as an enhancement of the westward auroral electrojet centered around local midnight (Akasofu et al., 1965; Heppner, 1954; Weimer, 1994). The detectability of this westward-directed ionospheric current connected to the SCW depends on the background conductivity of the ionosphere (El-Alaoui et al., 2023; Newell et al., 1996; Wang et al., 2005). This is in part due to the strength of the Hall current of the Cowling current channel, the signal detectable on the ground, modulated by the conductivity gradient created by the auroral precipitation from the substorm and the background ionosphere (Amm & Fujii, 2008; Boström, 1964; Cowling, 1932). Further out, magnetic reconnection creates an isolated plasmoid that is accelerated out and ejected from the magnetotail (Hones Jr, 1984). During the recovery phase, the magnetosphere returns to its quiet-time configuration, although complex auroral features are still observed in the ionosphere (Forsyth et al., 2020; Opgenoorth et al., 1994; Pulkkinen et al., 1994). During a complete cycle, the substorm is capable of processing up to $\sim 10^{15}$J of solar-origin energy (Tanskanen et al., 2002).

The magnetic perturbations measured on the ground can be rotated to equivalent current maps, for example, a positive northward magnetic deflection is produced by an eastward flowing ionospheric current. There must be a degree of care when interpreting these equivalent currents as gradients in conductivity, and the contribution of more distant currents than those in the ionosphere also affects the observed perturbations (Milan et al., 2017). However, from decades of study, the magnetic perturbations produced in the polar regions can be largely decomposed into two main characteristic patterns: the Disturbance Polar (DP) 1 and 2 patterns (Nishida & Kokubun, 1971). The DP1 pattern is associated with the ionospheric leg of the substorm current wedge (Akasofu et al., 1965), consisting of a strong westward-directed ionospheric current centered at midnight magnetic local time (MLT) (McPherron et al., 1973). The two-cell DP2 current pattern is produced by the convection of magnetic flux described by the Dungey cycle (Dungey, 1961). Its ground signature is detectable due to the Hall current eastward and westward electrojets in the afternoon and morning MLT sectors. It is highly correlated with the southward component of the interplanetary magnetic field (IMF), B_z, on short time scales and is associated with general magnetospheric convection. Shore et al. (2018), using data-driven methods on SuperMAG data, were able to decompose these two spatio-temporal patterns, in addition to patterns related to the DPY equivalent current system (Friis-Christensen et al., 1985; Friis-Christensen & Wilhjelm, 1975) and the NBZ field-aligned current system (Iijima et al., 1984; Maezawa, 1976), among the six modes that contribute most to the magnetic field variance throughout Solar Cycle 23. As shown by the Shore et al. (2018) analysis, the DPY spatial pattern is a single vortex that is approximately centered on the magnetic pole and whose polarity and strength is controlled by IMF By. When added to the symmetric component of the DP2 pattern, the DPY component controls the relative strength and shape of the two vortices of the DP2 pattern, creating the so-called "banana" and "orange" convection cells (e.g., Østgaard et al., 2018). The NBZ pattern appears as twin reversed lobe convection cells on the dayside polar cap and is associated with periods of purely northward IMF. Additionally, the reanalysis conducted by Shore et al. (2017) of the single month of February 2001, found that the amplitude of both the DP1 and DP2 modes increased rapidly at substorm onset.

A common way to identify substorms is to detect its ground perturbation due to the ionospheric westward current of the substorm current wedge (DP1 current pattern). By Ampere's law, this creates a southward magnetic deflection observable on the ground at auroral zone latitudes. Other methods of identifying substorms include leveraging auroral imagery, taken from spacecraft (Frey et al., 2004; Liou, 2010) or on the ground using all-sky imagers (Nishimura et al., 2010), or from particle injections observed by spacecraft at geosynchronous orbit (Borovsky et al., 1993; Borovsky & Yakymenko, 2017). Each method comes with its own advantages and disadvantages, such as identifying substorms from auroral features that currently require these features to be observable from the ground or when a spacecraft is suitably positioned to observe them. The advantage of using magnetic indices is the almost global coverage from the many magnetic observatories and arrays that have been deployed. However, it should be noted that the observation of one signature associated with the substorm does not confirm the occurrence of the phenomena and that any two different substorm signatures appear together for less than 50% of substorms (Lao et al., 2024).

The magnetic indices AU and AL (Davis & Sugiura, 1966), and their SMU and SML generalization to many stations (Newell & Gjerloev, 2011), were developed to trace the maximum and minimum northward deflections of the northward component of the geomagnetic field across a range of auroral latitude magnetometer stations. At substorm onset, a sharp negative bay is observed in the AL/SML index, indicating an enhancement of the westward auroral electrojet by the substorm. Many automated methods have recently been developed that take advantage of these indices to identify the onset of the expansion phase of the substorm (Borovsky & Yakymenko, 2017; Forsyth et al., 2015; McPherron & Chu, 2017; Newell & Gjerloev, 2011; Ohtani & Gjerloev, 2020). However, the substorm is not the only magnetospheric phenomenon capable of producing such enhancements of the westward electrojet (Kamide & Kokubun, 1996). In particular, during periods of enhanced convection, DP2 is enhanced, and there is an enhancement in both the eastward and westward electrojets. Thus, SML automated methods may be contaminated with false positive events. Of the techniques mentioned above, it is only the method of Forsyth et al. (2015) that attempts to explicitly separate the DP2 signature of enhanced convection from substorms by assessing periods in which the SML and SMU enhancements are similar.

In this study, we examine the **S**ubstorm **O**nsets and **PH**ases from **I**ndices of the **E**lectrojets (SOPHIE) technique developed by Forsyth et al. (2015), where they attempt to distinguish between the ground signatures of substorms, which are believed to only enhance the equivalent currents of the DP1 pattern, and periods of enhanced convection due to enhancements of the DP2 current pattern, which are well correlated with periods when the solar wind directly drives the magnetosphere. We quantify the two current pattern contributions to substorm-like SML intensifications across all magnetic local times. In addition to this, we explore the parameter space used for filtering out these convection enhancements from "true" substorms, to evaluate the effectiveness of auroral indices for substorm identification.

2. Data and Method

2.1. SOPHIE Identification of Substorm Events

SOPHIE is a nonparametric technique applied to the auroral indices SML and SMU to identify phases of the substorm cycle at a temporal resolution of 1 min (Forsyth et al., 2015). The SOPHIE technique for identifying the phases of the substorm has been used extensively in the literature, particularly in statistical studies of the effects of substorms, including studies of the magnetotail lobes (Coxon et al., 2018), radiation belts (Forsyth et al., 2016; Rodger, Clilverd, et al., 2022; Rodger, Hendry, et al., 2022), ring current (Sandhu et al., 2019), field-aligned currents (Coxon et al., 2017), ground-induced currents (Freeman et al., 2019; Smith et al., 2024), and auroral kilometric radiation (Waters et al., 2022), as well as the influence of the solar wind and interplanetary magnetic field on substorms (Laitinen et al., 2024; Lockwood, 2023; Walker et al., 2024).

Precisely, SOPHIE identifies substorm expansion phase onsets using an expansion phase threshold (EPT) based on the yearly percentile rates of decrease of the SML index. The substorm recovery phase is identified similarly, so that the difference in the number of expansion phases and recovery phases is minimized. The authors then argue that any period that is not part of an ongoing expansion or recovery phase can be labeled as a potential growth phase, in which magnetic flux and energy is stored in the magnetotail. In addition, Forsyth et al. (2015) considered that not all decreases and recoveries of SML are driven by substorms and that similar signatures may arise due to enhancements in magnetospheric convection. To address this, if the magnitude of the overall rates of change of SML and SMU during an identified expansion phase is within a factor of 2, that expansion phase and its following recovery phase are flagged as a Convection Enhancement. For full details on the SOPHIE technique, please refer to the original manuscript (Forsyth et al., 2015). In this study, we examine the period between January 1997 and December 2019 inclusive using SOPHIE or EPT 90, such that for an SML-bay to be considered a candidate substorm onset, the gradient of its decrease must surpass the 90th percentile of negative gradients observed in that calendar year. This threshold of SOPHIE has been shown to have the best association with other substorm onset lists (Lao et al., 2024).

As the SOPHIE technique does not dictate the ordering of substorm phases, onsets of the expansion phase can occur following growth or recovery phases. In this study, we classify an event as an isolated substorm if it follows the phase ordering of Growth-Expansion-Recovery-Growth. In Figure 1, two isolated events are shown between 17:30 UT on 1997/01/10 and 02:00 UT on 1997/01/11. Here, the first isolated event has its growth phase beginning around 17:30 UT with the expansion onset occurring at 18:50 UT followed by a recovery phase at 19:02 UT transitioning into another growth phase at 20:41 UT. Isolated substorms occur frequently in SOPHIE EPT 90 event identification, compromising 54% of all expansion phase events between January 1997 and December 2019.

The SOPHIE technique can also resolve periods of compound or recurrent substorm activity (e.g., Rodger, Hendry, et al. (2022); Rodger, Clilverd, et al. (2022); Sandhu et al. (2019)). These periods are characterized by multiple expansion and recovery phases, with no intermediate growth phase between them. An example of such a period is shown in Figure 1, with the first onset of the compound event occurring at 16:05 UT on 1997/01/10 and the second at 16:41 UT. The period of compound activity is ended by the occurrence of a growth phase at 17:28 UT. All onsets in a compound sequence are classified as individual compound substorms, even though the first onset follows from a growth phase. For SOPHIE EPT 90, 27% of expansion phase events are compound substorms between January 1997 and December 2019, although lower EPTs tend to identify more compound events (Forsyth et al., 2015).

As described earlier, SOPHIE uses the SMU index for information to filter out events that are not due to substorm activity. The technique accomplishes this by flagging expansion phases in the time series where the change in SMU is similar to what is observed in |SML|. Specifically, expansion phases that have a change in |SML| less than twice that of the change in SMU, that is, $|dSML_{expansion\ phase}|/|dSMU_{expansion\ phase}| < 2$, are flagged as potentially misidentified substorms due to enhancements in convection. The following recovery phase after the expansion is also flagged. In the process of completing this study, we found that the SOPHIE technique mislabeled certain substorm cases as convection enhancement intervals. These cases were when a negative SML bay formed and a

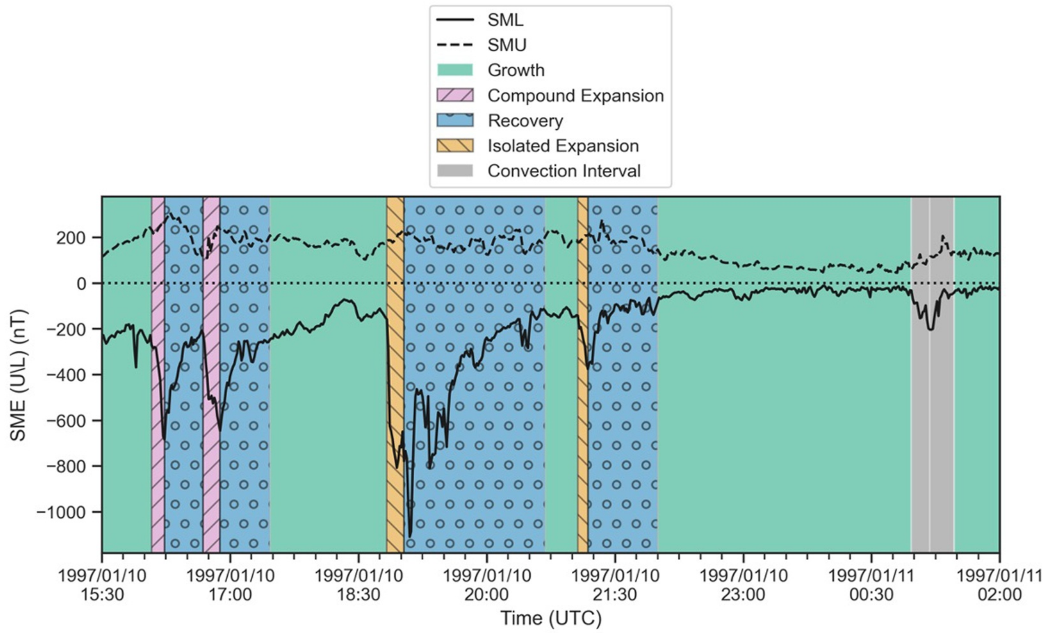

Figure 1. The SML (Solid Black) and SMU (Dashed Black) indices (nT) plotted as a function of time, with the background color indicating the substorm phase identified by the Substorm Onsets and Phases from Indices of the Electrojet (SOPHIE) technique for that period. Green indicates periods of growth, orange ∖-hatched corresponds to expansion phase that is part of an isolated substorm, pink /-hatched corresponds to an expansion phase that is part of a compound substorm, blue ∘-hatched indicates a recovery phase and gray corresponds to periods that have been identified as convection enhancement intervals.

decrease was also observed in SMU that met the criteria above. If we consider that SMU is generally reflective of the strength of convection, a plausible explanation that a decrease in SMU can be observed during an expansion phase is the scenario that the substorm occurs in the subsequent period after a northward turning in the IMF, such that dayside reconnection rate and therefore the strength of the convection decreases. As we would normally expect SMU to increase, rather than decrease, during convection enhancements, we have revised the criteria for a Convection Enhancement to be as follows.

1. $\Delta SMU > 0$ over the expansion interval.
2. $\Delta SML < 0$ over the expansion interval.
3. $\frac{-\Delta SML}{\Delta SMU} < 2$ over the expansion interval.

If these three criteria are satisfied, then the expansion phase and the following recovery are flagged as a convection enhancement. Figure 1 shows an example period that has been flagged by the amended SOPHIE technique, with the event beginning at 02:07 UT on 1997/01/11 and ending at 02:40 UT. Here, the flagged expansion phase lasted 15 min. In the period analyzed, 8% of the identified expansion events were flagged as possible convection enhancement intervals. All the analysis conducted in this study was completed with this new corrected logic of SOPHIE when filtering convection enhancements from substorms.

In the original SOPHIE paper (Forsyth et al., 2015), the factor of two used in the convection enhancement criterion 3 above was not fully explored but rather based on expert judgment, which is not uncommon in solar-terrestrial physics (e.g., the Newell and Gjerloev (2011) identification of substorm onset as being when dSML/dt is less than −15 nT/min or the identification of geomagnetic storms as when Dst drops below −50 nT). For symmetric DP2 electrojets, then the convection enhancement factor in criterion 3 would be unity, which might approximate a summertime case where the morning and afternoon MLT sectors are similarly illuminated by the Sun and have similar conductances. However, electron precipitation from substorm injections can sustain an enhanced morning MLT conductance (e.g., Wallis and Budzinski (1981)) and create a relatively stronger westward DP2 electrojet, as is statistically observed (Shore et al., 2018). Thus, a factor of two is again chosen in criterion 3 to take account of this, but we shall later explore the effect of varying this factor in Section 3.4.

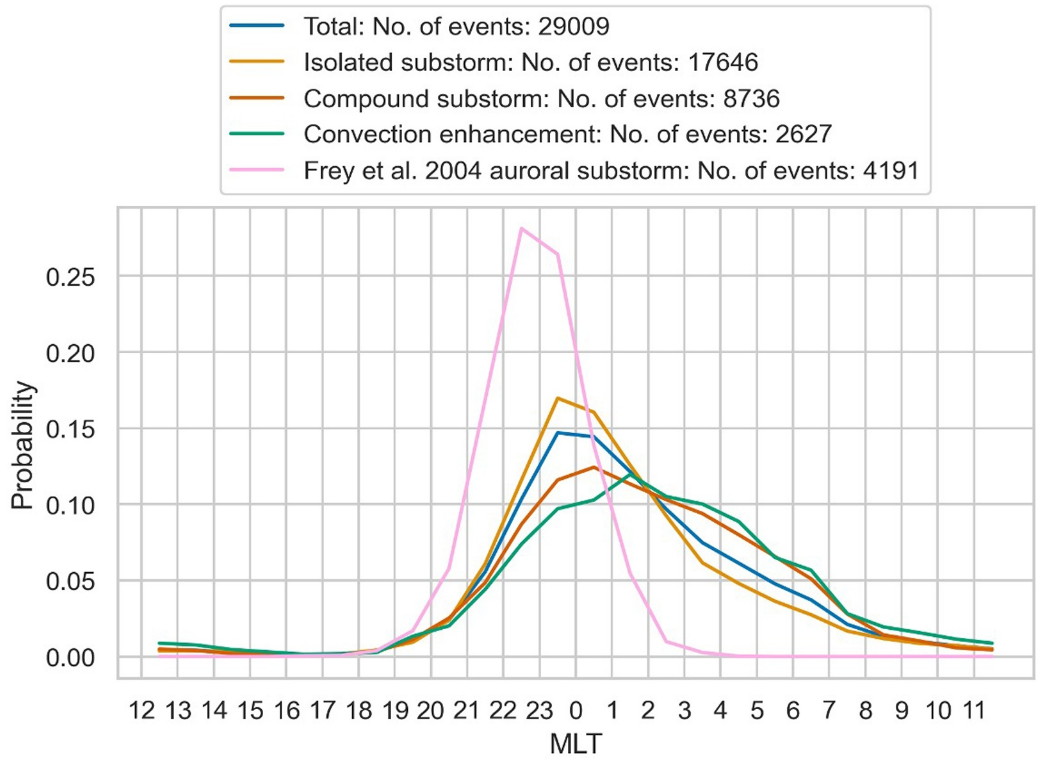

Figure 2. The magnetic local time (MLT) probability distribution of the contributing station to SML for different event types. The blue indicates the total event distribution, orange corresponds to the isolated substorm events, red corresponds to the compounds substorm events, and green corresponds to the convection enhancements.

2.2. MLT Distributions of Events

Figure 2 shows the probability distributions of the onset magnetic local time (MLT) of each SOPHIE EPT 90 event type discussed in Section 2.1. That is, from the SOPHIE EPT 90 substorm phase list in the period January 1997 to December 2019 inclusive, we identified the subsets of isolated substorms, compound substorms, and convection enhancements and, for each subset, the MLT of the station that contributes to SML at the time of event onset was sorted into a corresponding 1-hr MLT wide bin. For example, the first compound onset in Figure 1 at 16:05 UT has its contributing station at 21.75 MLT at the onset of the expansion phase, and therefore this occurrence would be placed in the 21–22 MLT bin. The probability distribution of the onset MLT for each event type was then calculated by dividing the number of events of a given type in each MLT bin by the total number of events of that type. Similarly, Figure 2 also shows the probability distribution of the MLT of substorm onsets identified by Frey et al. (2004) from auroral images in the period from 19 May 2000 to 31 December 2002 inclusive.

Figure 2 shows that the probability distributions of different SOPHIE EPT 90 event types are somewhat different from each other and to that of the Frey et al. (2004) auroral events. Firstly, the MLT distribution of auroral events (shown in pink) peaks 1 hr of MLT earlier than that of the SOPHIE isolated substorm events (shown in gold). As discussed further in Sections 3 and 4, this westward displacement is likely explained by the localized auroral brightening signature of substorm onset identified by Frey et al. (2004) being associated with the upward field-aligned current that sits at the western end of the DP1 substorm electrojet detected by SOPHIE.

Secondly, the isolated substorm distribution is asymmetric with a more eastward extended tail than the symmetric auroral distribution. Whilst, as argued above, an eastward shift of the isolated substorm distribution is to be expected, we hypothesize that its MLT asymmetry is because some SOPHIE enhanced convection events are falsely identified as isolated substorms. The convection enhancement distribution (shown in green) is a broad, approximately symmetric, distribution centered later at 01–02 MLT. As will be shown in the next section, the MLT extent of this distribution is consistent with the extent of the westward electrojet of the DP2 ionospheric equivalent current pattern, which the SML index is expected to be sampling during periods when magnetospheric convection is enhanced. Thus, if some convection enhancements are misidentified as isolated substorms, then these anomalous events will be predominantly in the post-midnight MLT sector, and the isolated substorm distribution will be erroneously skewed eastward, as observed.

Thirdly, the compound substorm distribution is intermediate between the isolated substorm distribution and the enhanced convection distribution. Thus, the above hypothesis suggests that the compound substorm distribution is even more contaminated by misidentified enhanced convection events than the isolated substorm distribution. This is plausible because the SOPHIE definition of an isolated substorm is most similar to the classic three-phase description of the substorm and is stricter than that of the compound substorm (i.e., an isolated substorm onset requires a preceding growth phase, whereas each compound substorm onset does not).

In summary, we hypothesize that the isolated substorm distribution in Figure 2 is a weighted sum of the MLT distribution of true substorms and the MLT distribution of some misidentified enhanced convection events. In the next section, we attempt to separate out the true substorm distribution.

3. Results

3.1. Decomposition of MLT Distributions

As noted above, the probability distribution of the MLT of isolated substorm onsets identified by the SOPHIE EPT 90 technique shares some similarities with the probability distribution of the MLT of auroral onsets from Frey et al. (2004) and some similarities with the probability distribution of the MLT of enhanced convection onsets from SOPHIE. We thus postulate that the SOPHIE technique has misidentified some enhanced convection events as isolated substorms, and thus the histogram of the MLT of SOPHIE isolated substorm onsets is a combination of the histograms of the MLT of true DP1 substorm onsets and DP2 convection enhancements.

We seek to isolate the DP1 histogram by estimating the DP2 histogram and removing it from the SOPHIE isolated substorm histogram. To estimate the DP2 histogram, we rescale the histogram of the MLT of SOPHIE convection enhancements by multiplying the corresponding probability distribution shown in Figure 2 by increasing integer values until the number of convection enhancements in any bin exceeds the number of isolated substorm events from SOPHIE in that bin. The estimated DP2 histogram is shown by the dashed-dot green line in Figure 3 and the SOPHIE isolated substorm histogram is shown by the solid gold line. The rescaling assumes that there exists some MLT where DP2 enhancements exclusively occur and no DP1 substorm onsets occur. We then subtract the estimated DP2 histogram from the SOPHIE isolated substorm histogram to yield the estimated histogram of the MLT of true DP1 substorm onsets, shown by the dashed-dotted gray line. It is lacking the post-midnight MLT "bump" and has a shape similar to the Frey et al. (2004) onset distribution but shifted eastward.

3.2. Interpretation of the Decomposition Results

Figure 4c shows the resulting probability distributions of the DP1 and DP2 enhancements, with the DP1 distribution transformed into a PDF using the same method of dividing each MLT bin by the total number of events. Additionally, the MLT probability distribution of the Frey et al. (2004) auroral onsets is also plotted. Shown in Figures 4a and 4b are the Shore et al. (2018) empirical orthogonal function (EOF) representations of the DP1 and DP2 equivalent current patterns from a reanalysis of the Northern Hemisphere surface external and internal magnetic field during Solar Cycle 23. In these subplots, increasingly red (blue) indicates a larger southward (northward) magnetic deflection observed on the ground due to the DP1 and DP2 current patterns. Below the Onset MLT probability distributions, are the spatial amplitude profiles from auroral latitudes ($65^\circ - 75^\circ$ MLat) of the DP1 pattern and DP2 pattern (d) of Shore et al. (2018), where greater than zero indicates the contribution to a southward magnetic deflection and less than zero indicates the contribution to a northward magnetic deflection, the concentric rings on (a) and (b) indicate the latitudes from which we derived the profiles. The spatial amplitude profiles seen in Figure 4d are the mean of the latitudinal profiles between the two rings in Figures 4a and 4b. The spatial resolution of the Shore et al. (2018) profiles increases as the latitude decreases, that is, there are more dots in each concentric ring that go away from the center; therefore, each latitudinal profile between $65^\circ - 75^\circ$ MLat was resampled to a 1 MLT resolution grid centered on the half-hours of each MLT before taking the mean.

Figures 4c and 4d show that the extent of the probability distributions for the location of the DP1 and DP2 events is in good agreement with the extent of the southward deflections of the DP1 and DP2 Spatial Amplitude profiles

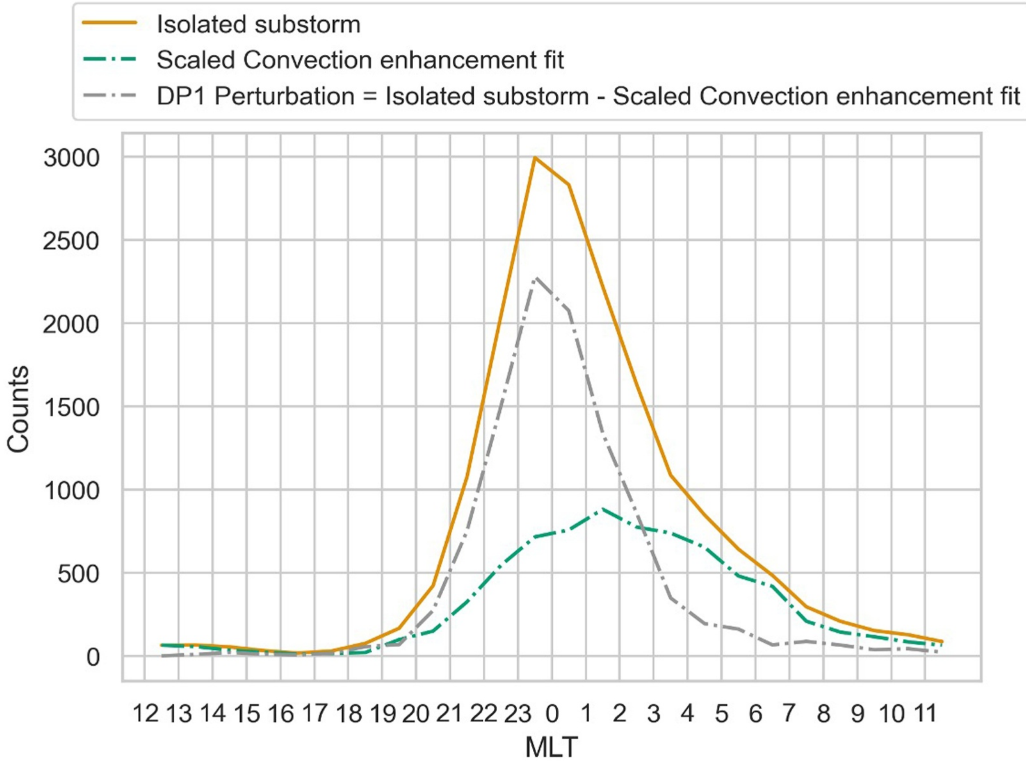

Figure 3. The Onset MLT histogram of the Isolated substorms (Orange), the Scaled Convection enhancement distribution (Dashed-Dot Green) and the residual distribution when subtracting the Scaled Convection enhancements from the Isolated substorms (Dashed-Dot Gray).

across the auroral latitudes. This result validates the decomposition of SML-bay events into DP1 and DP2 contributions, since the bulk of each event distribution lines up with the region of maximal southward magnetic deflection (that sampled by the SML index) from each spatial pattern. The DP1 Spatial Amplitude profile differs from the DP1 perturbation probability of occurrence on their duskward edge, with a non-zero contribution to southward magnetic deflections from the DP1 patterns still observable around ∼18MLT. However, since these are spatial profiles of north-south magnetic deflections, we do not expect a one-to-one correspondence to probabilities of event occurrence.

The probability distribution of the DP1 perturbation is more akin to the auroral onsets than the isolated substorms originally identified, sharply peaking before midnight (0.28 at 22–23 MLT for Frey et al. (2004) and 0.22 at 23-00 MLT for the resolved DP1 perturbations) and rapidly dropping to zero in the afternoon and morning MLTs. We note that there is an offset of 1 hr MLT east for the DP1 probability distribution compared to the Frey et al. (2004) distribution. This is likely due to the auroral signature originating near the westward edge of the Substorm Current Wedge, where the downward-propagating electrons provide the upward field-aligned current, whereas the SML signature originates from a horizontal current connecting the eastward and westward legs of the substorm current wedge. It should be noted that the probability distribution of the onset MLTs and the positive amplitudes of the Spatial Amplitude profiles of the DP1 and DP2 events overlap in the midnight sector. As such, magnetic deflections in this region could be due to enhancements related to either current pattern, complicating the identification of substorms.

3.3. Decomposition of Other SOPHIE EPT 90 Event Types

As mentioned in Section 2.1, in addition to isolated substorms and enhanced convection events, the SOPHIE technique also identifies compound substorms whose onset need not be preceded by a growth phase. Furthermore, as SOPHIE identifies the timing of the recovery phases nonparametrically, similarly to how it identifies expansion phases, and does not enforce that an expansion phase is directly followed by a recovery, other event types are also

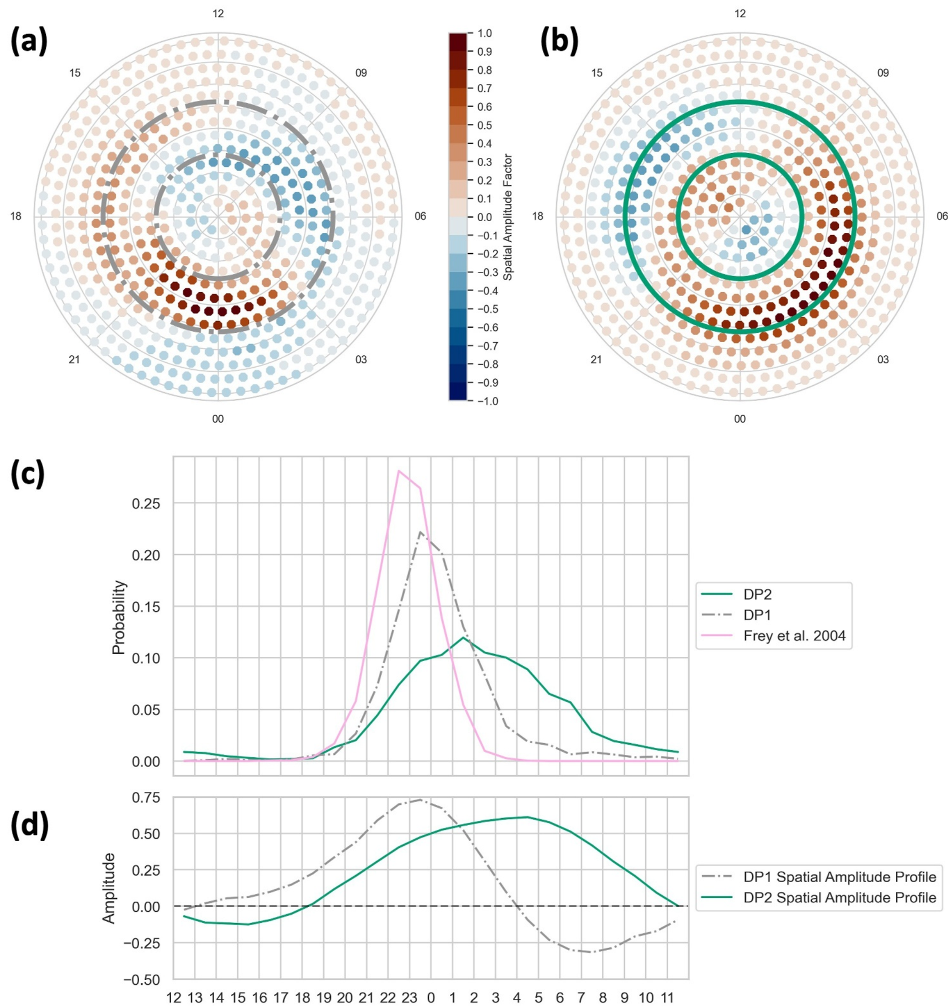

Figure 4. The DP1 (a) and DP2 (b) spatial patterns obtained by Shore et al. (2018). In these figures, the darker color indicates a greater amplitude of the deviation to the θ component ground magnetic field, with red indicating a southward deviation and blue northward. Subplot (c) shows the Onset MLT distributions obtained from the analysis of the SOPHIE technique in this study. In addition to the obtained DP1 (Dashed-Dot Gray) and DP2 (Solid Green) perturbation distributions, the Frey et al. (2004) auroral substorm Onset MLT distribution is also plotted in pink. Subplot (d) shows the mean amplitude of the DP1 (Dashed-Dot Gray) and DP2 (Solid Green) patterns at auroral latitudes by MLT, these profiles were obtained by taking longitudinal cuts of the Shore et al. (2018) profile.

possible. One of these event types occurs in an order in which an identified expansion has no counterpart recovery but instead proceeds immediately into a growth phase, following a Growth-Expansion-Growth regime. Furthermore, recovery phases may be placed before an expansion phase following an isolated substorm regime, following a Growth-Recovery-Expansion-Recovery-Growth order. These events, which we have labeled Other substorms, account for 3,061 additional events between January 1997 and December 2019 (0.09% of all SOPHIE EPT 90 events) or an additional ~ 130 events per year. The occurrence of these events shows a trend similar to that of the Solar Cycle (not shown), but their occurrence is not explored in this study. Furthermore, SOPHIE-identified substorms may occur recurrently after a SOPHIE-identified convection enhancement similar to the compound example shown in Figure 1, where the first expansion phase and associated recovery are instead a convection enhancement and the second event an identified substorm expansion and recovery. We have labeled any expansion phase events occurring directly after a convection enhancement without an intervening growth phase as an After Convection substorm. Note that a convection enhancement may occur during a set of compound events, thus splitting the series into two, with the events of the first part labeled as compound substorms and the events after the convection enhancement labeled as After Convection substorm. There are 886 events classified as After Convection Onsets between January 1997 and December 2019 (0.03% of all SOPHIE EPT 90 events).

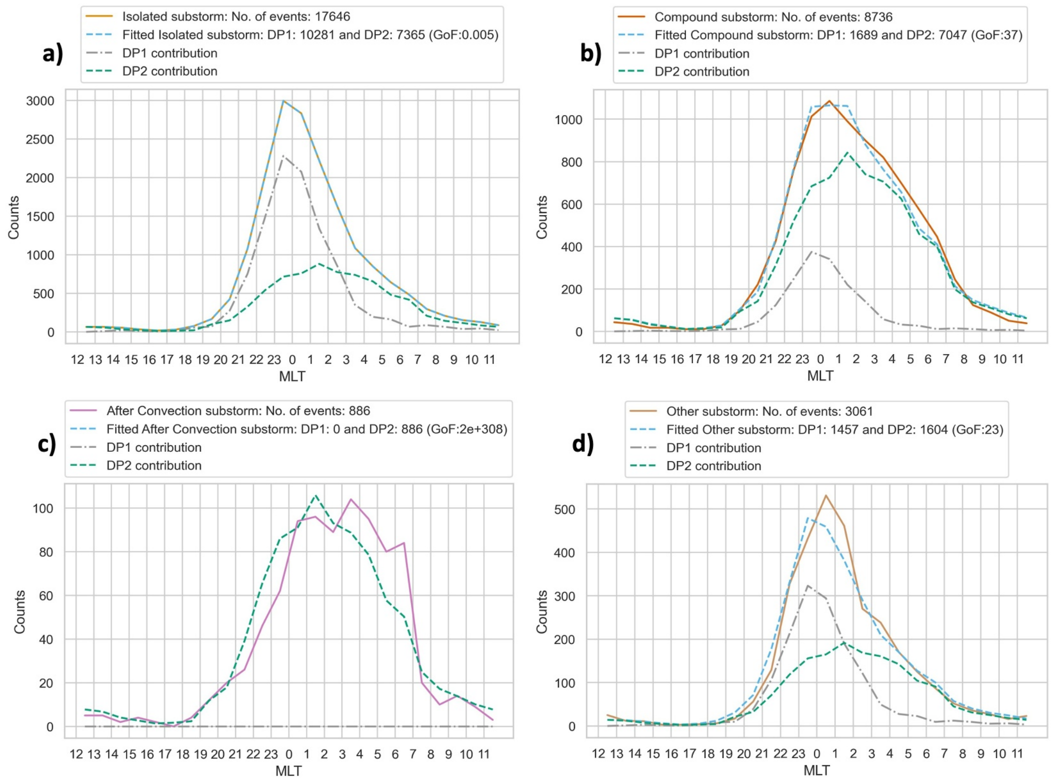

Figure 5. The reconstruction of MLT distributions of the full spectrum of SOPHIE event types using the obtained DP1 and DP2 MLT distributions from Figure 4. (a) Reconstruction of the isolated substorms, (b) the reconstruction of compound substorms, (c) the reconstruction of substorm expansion phases that directly follow on from a convection enhancement and (d) the reconstruction of substorms that do not fit into the other categories.

Using the decomposed MLT probability distributions of DP1 and DP2 to fit the onset MLT histograms, it is possible to evaluate the contribution of DP1 and DP2 to the different types of events that populate the SOPHIE EPT 90 phase list. The results of the fitting are shown in Figure 5, where we have fit the four different SOPHIE substorm types (Isolated substorms (panel a), Compound substorms (panel b), After Convection substorms (panel c) and Other substorms (panel d)). The fitting was completed by using a linear combination of the DP1 and DP2 probability distribution functions, scaled so that the sum of their scaling must equal the number of events of the fitted SOPHIE event type. For example, when fitting the Compound substorms, the combinations that were evaluated were $0 \times pdf(DP1) + 8736 \times pdf(DP2)$, $1 \times pdf(DP1) + 8735 \times pdf(DP2)$, $2 \times pdf(DP1) + 8734 \times pdf(DP2)$, …, $8736 \times pdf(DP1) + 0 \times pdf(DP2)$. The quality of the fits was evaluated by calculating a goodness of fit value for each fit carried out with the parameter used in this study being the chi-square value given by

$$\chi^2 = \sum_{i}^{N} \frac{\left[y_i^{\text{meas}} - y_i^{\text{model}}(\mathbf{v})\right]^2}{\epsilon_i^2}$$

where y_i^{meas} is the count observed in each MLT of the original distribution, y_i^{model} is the count evaluated in each MLT bin of the fitted distribution, and ϵ_i is the estimated uncertainty in the data. In the study conducted, we take ϵ_i as the standard error of the count in each MLT bin, that is, it is the square root of the count based on Poisson counting statistics. The combination that had the lowest chi-square value was selected as the best fit, in the case of the Compound substorms, this was the linear combination $1689 \times pdf(DP1) + 7047 \times pdf(DP2)$, which had a chi-square of 37.

The reconstruction of the distribution for each type of event is shown as a cyan dashed line in each subplot of Figure 5, and with the chi-square goodness-of-fit value for the reconstruction in the legend of each subplot. There

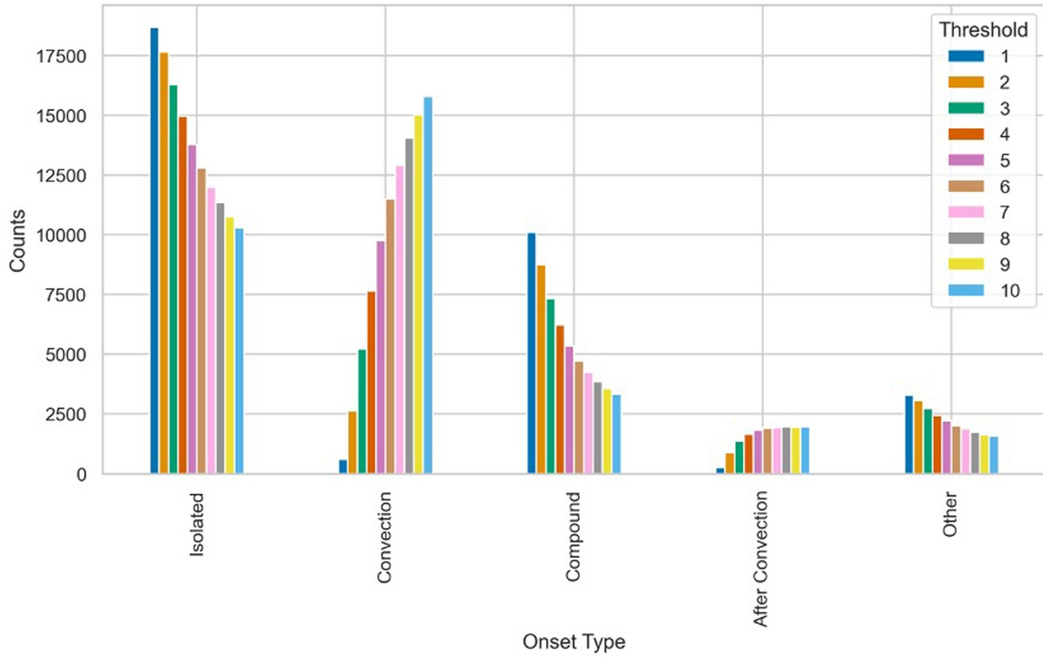

Figure 6. Event numbers identified by the SOPHIE technique as the threshold value for identifying convection enhancements is modified. A value of 2 means that for a given event, the absolute rate of decrease in SML must be more than twice that of the rate of increase in SMU to be classed as a substorm rather than a convection enhancement. Previously published SOPHIE lists have used a threshold of 2.

is no desired threshold for this value; however, the "best fit" by the linear combination of DP1 and DP2 probability distributions for each SOPHIE event reconstruction was selected by minimizing the chi-square goodness-of-fit. The distribution that is best fit by a combination of the DP1 and DP2 distributions is the isolated substorms, shown in Figure 5a, with a chi-square goodness of fit value of 0.005. However, this is to be expected, as this is the distribution from which we decomposed the DP1 events. The worst fit is to the Onset MLT distribution of After Convection onsets, shown in Figure 5c, with a chi-square goodness-of-fit value orders of magnitude larger than the other distributions being fitted and for which the peak at 4 MLT is not reproduced. As a result of the fitting, we can distinguish the number of events due to DP1 or DP2 for each SOPHIE event type. For example, of the 17,646 isolated substorm events, between January 1997 and December 2019, 10,281 were identified due to enhancements of the DP1 current pattern, and the remaining 7,365 due to an enhancement of DP2. Taking the sum of all event types and the DP1 and DP2 current pattern contributions to these, including those originally identified as convection events, we find 32,956 westward electrojet enhancement events between January 1997 and December 2019 (~ 1430 events per year). SOPHIE originally categorized these into 30,329 substorms (92% of events) and 2,627 convection enhancements (8% of events). With our decomposition, we find that 41% or 13,427 events are due to enhancements of the DP1 current pattern (~ 590 events per year) and 59% or 19,529 are due to enhancements of DP2 (~ 840 events per year).

3.4. Sensitivity of the Decomposition to the Detection Threshold for Convection Enhancement Events

As discussed in Section 2.1 above, both the original SOPHIE technique and the amended technique used here employ an author-set threshold to decide which SML bays are due to enhanced convection rather than substorm expansion. Currently, this threshold has a value of two based on expert judgment, as discussed above in Section 2.1, but now we examine the sensitivity of substorm and convection enhancement identification to this value.

Figure 6 shows the breakdown of SOPHIE event types for integer values of the convection event threshold between unity and ten (a table with the underlying data is included in Supporting Information S1). We observe that 32,956 SML bay events are identified between January 1997 and December 2019, invariant of the convection event threshold used. The division of these 32,956 events identified into the five types of events varies significantly as the threshold increases. Note that threshold 2 corresponds to the MLT distributions plotted in Figure 2,

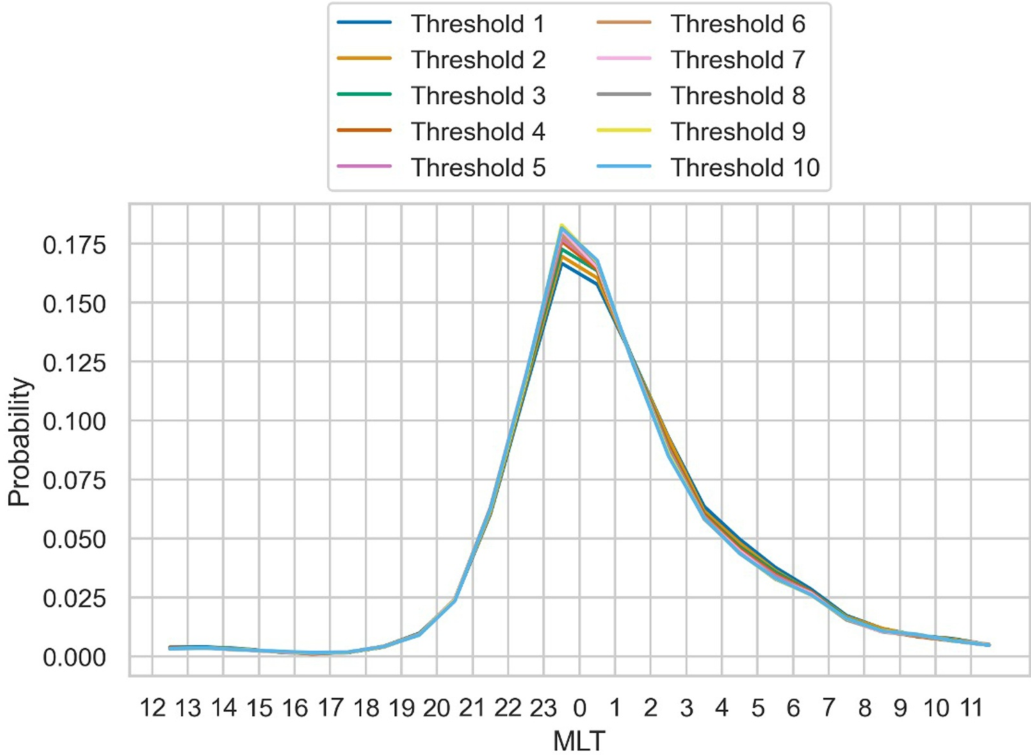

Figure 7. Isolated Substorm probability distribution for various convection event filtering thresholds used.

without the After Convection and Other substorms. As expected, more events are classified as convection enhancements than substorms as the convection event threshold increases, since the magnitude of the change in SML required for an event to be labeled as a substorm becomes greater. We observe that convection events make up less than 2% of the events when using a threshold value of 1. This increases to 48% when using a threshold value of 10. Similarly, the number of After Convection substorms increases as the convection event threshold is increased, although this number seemingly saturates at 6% of events at a threshold of 7 and above. As the number of identified substorms decreases as the threshold increases, this does not happen homogeneously across isolated and compound substorms that reduce at different rates. Compared to their Threshold 1 value, isolated substorms have reduced by 45% when using a Threshold of 10, whereas compound substorms have reduced by 67%, an indication that compound events have a higher degree of DP2 contamination than isolated substorms.

Figure 7 shows the Onset MLT probability distributions for isolated substorms identified using different convection enhancement thresholds. We observe that these probability distributions continue to show additional events in the morning MLTs as the threshold for the convection enhancement classification increases, though there is a marginal increase in the peak at 23-00 MLT (∼0.01 difference between thresholds 1 and 10). This implies that varying the convection enhancement threshold is insufficient to reduce the number of DP2 events classified as isolated substorms.

The decomposition of events into contributions from DP1 and DP2 described above in Section 3.1 was applied to the distributions of each threshold. This was completed using the Isolated substorm and Convection enhancement MLT probability distributions evaluated for each threshold (not shown). Similarly to Section 3.1, the four substorm event types (Isolated substorm, Compound substorm, After Convection substorm, and Other substorm) were divided into their underlying DP1 and DP2 current pattern contributions. Figure 8 shows the split of the events identified by the SOPHIE technique into originally identified substorms and convection enhancements. We also show the relative contributions of DP1 and DP2 that result from the fitting described above reapplied to the subsets of substorm and convection events for each threshold. Note that previously published event lists derived from the SOPHIE technique correspond to the SML/SMU Threshold of 2. As discussed above, we

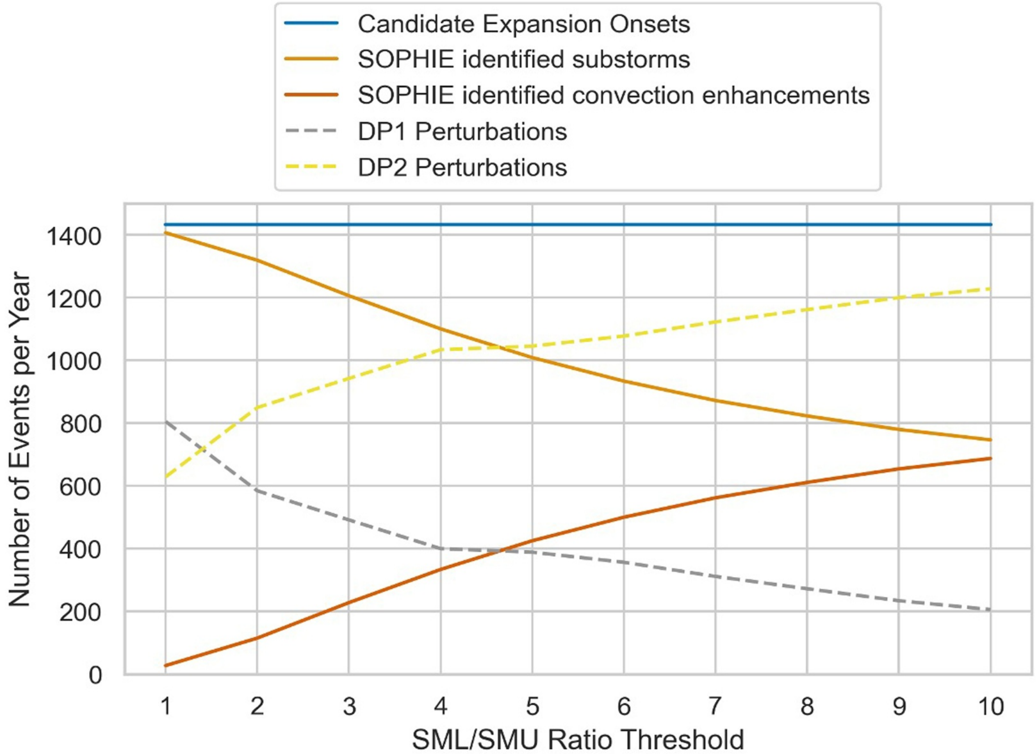

Figure 8. Numbers of substorms and convection enhancements originally identified by SOPHIE (Solid) and also their breakdown into DP1 or DP2 (Dashed) as a function of threshold used for convection enhancement filtering. Blue corresponds to the number of candidate expansion phases identified that is, all periods which satisfy the SOPHIE EPT 90 condition of a decrease in SML that exceeds that 90th percentile of the yearly decrease in SML. Orange corresponds to the number that were identified as a substorm, red corresponds to the number of candidate events identified as a convection enhancement interval, dashed gray corresponds to the number of all candidate events that were due to the DP1 pattern, and dashed yellow corresponds to the number of all events that were due to the DP2 pattern.

observe the trend of more events being classed as convection enhancements rather than substorms as the threshold value increases. Additionally, as the threshold increases, more events are classified as DP2 rather than DP1.

We observe that the number of SOPHIE identified substorms and DP1 perturbations do not intersect or converge for any value of the convection enhancement threshold. The number of events due to enhancements of the DP1 equivalent pattern is always less than the number of SOPHIE identified substorms; as such, the contributions of DP1 and DP2 can always be decomposed from the MLT distribution of SOPHIE substorm events. This implies that SOPHIE identified substorms are not solely due to enhancements of the DP1 current (or the closure of the Substorm Current Wedge through the ionosphere), regardless of the threshold value used. However, while there is some contamination of SOPHIE identified substorms by convection enhancement events, this contamination is likely greater for other methods that make no attempt to identify events with enhancements in SMU.

4. Discussion

In this study, we have examined the contribution of enhancements of the DP1 and DP2 current patterns to substorm-like SML bays by inspecting event MLT distributions as identified by the SOPHIE technique (Forsyth et al., 2015). Our results indicate that there is a notable contribution to substorm-like SML bays due to enhancements of the DP2 current pattern. Moreover, as SOPHIE is only one of many techniques applied to the AL/SML index for substorm identification, albeit one that attempts to filter by leveraging the SMU index also, any technique using these indices will be populated with "DP2 events."

To decompose the contribution of the DP1 pattern to SOPHIE identified substorms, we have assumed that SOPHIE convection enhancement events are a good proxy for enhancements of only the DP2 equivalent current pattern. The enhancement of the westward electrojet related to the DP2 pattern is largely expected to occur at morning MLTs; however, the work of Shore et al. (2018) shows that the enhancement of the westward electrojet due to DP2 can also occur in the midnight MLT sector. In agreement with this, Figure 3 shows that both the DP1 and DP2 events have non-zero probabilities of occurrence at night-side MLTs, with the extent of the SOPHIE convection events (green line of Figure 4c) matching the extent of the spatial amplitude profile of DP2 resolved by Shore et al. (2018) at auroral latitudes (Figure 4d). Moreover, SOPHIE makes use of the SMU index sampling the eastward electrojet to identify convection enhancements and, as it is unlikely for the formation and closure of the SCW to produce an enhancement of current in an eastward direction, we can be confident that the convection enhancements are due to enhancements of DP2 only and are minimally "contaminated" DP1-type events.

We have also assumed that substorms would primarily cause magnetic perturbations consistent with those of equivalent currents of the DP1 current pattern, with the formation of the substorm current wedge that closes through the ionosphere driving the enhancement of the westward electrojet (McPherron et al., 1973). This assumption is evidenced by the similarity of the decomposed DP1 distribution to that of auroral substorm onsets, as identified by Frey et al. (2004) and the extent of this distribution (gray dashed line in Figure 4c) that matches the extent of the spatial profile of the Shore et al. (2018) DP1 pattern from auroral latitudes (Figure 4d). The work of Shore et al. (2018) found that this pattern showed a sharp increase in amplitude at the onset of the substorm, was poorly correlated with the IMF B_z, and was never the dominant spatial mode contributing to ground magnetic field variance over a whole month during Solar Cycle 23, consistent with the interpretation of the substorm being a loading-unloading phenomenon of the magnetosphere.

There is a systematic shift between the observed MLT distributions, with the auroral onsets peaking 1 MLT westward of the SML identified onsets. This is consistent with the aurora being colocated with the upward FAC of the SCW, with the current carried by downward traveling electrons, while the peak southward ground magnetic perturbation is due to the westward flowing ionospheric current. Recent studies have indicated that the onset of auroral beads, one of the first auroral signatures of substorms (Kalmoni et al., 2017; Nishimura et al., 2016), coincides with ULF magnetic pulsations on the ground (Rae et al., 2012; Smith et al., 2020). However, these pulsations appear to be distinct from the large-scale perturbations that result in negative bays in AL/SML.

As we would expect the enhancement of the eastward electrojet to be correlated with that of the westward electrojet during periods of enhanced convection and uncorrelated during a substorm expansion, we explored the capability of using the SMU index within the SOPHIE technique to distinguish between non-substorm and substorm-related changes in SML. In Section 3.4, we tested various thresholds to filter out convection enhancements from substorms. Figure 8 indicates that regardless of the value of the threshold used to classify convection enhancement intervals or DP2 events, the number of identified substorms and DP1 events does not converge, which means that there is still a contribution of the DP2 pattern regardless of the selected threshold. This has two significant implications: (a) even when leveraging SMU/AU, the auroral indices alone are unable to distinguish the substorm from other magnetospheric phenomena; (b) the substorm can produce enhancements of the westward electrojet, at MLTs much different from the expected location of DP1. This could be due to localized conductivity enhancements in the ionosphere, either from the propagation of precipitated particles superposing with solar illumination (particularly during the Northern Hemisphere summer) or increased precipitation at these locations, further complicating the identification of true positive substorm events.

Isolated substorm studies using the Polar Ionospheric X-ray Imaging Experiment (PIXIE) by Østgaard et al. (1999) observed that the precipitation of the high-energy electrons that cause the X-ray aurora has a localized maximum toward morning magnetic local times (5–9 MLT). The authors noted that this localized maximum was delayed in response to the onset of the substorm, with the physical interpretation that these precipitating electrons have drifted from the injection region in the midnight sector before being scattered into the loss cone in the dawn sector. This precipitation will lead to an increased conductivity in the ionosphere, and as the westward convection electrojet is already colocated at morning MLTs, one can imagine a situation where the current flowing is increased and as a result producing a magnetic signature similar to the substorm negative bay in SML at a location unusual for a true positive identification from ground magnetometer data. However, since the precipitation was due to the substorm process, it would be misleading not to identify such an event as a substorm, although the enhancement of SML was not due to the closure of the substorm current wedge via the ionosphere. This resultant signature would be dependent on the timing and rate of ionization, and as such there is more to be explored between the relationship of the Substorm X-ray aurora and ground magnetic perturbations.

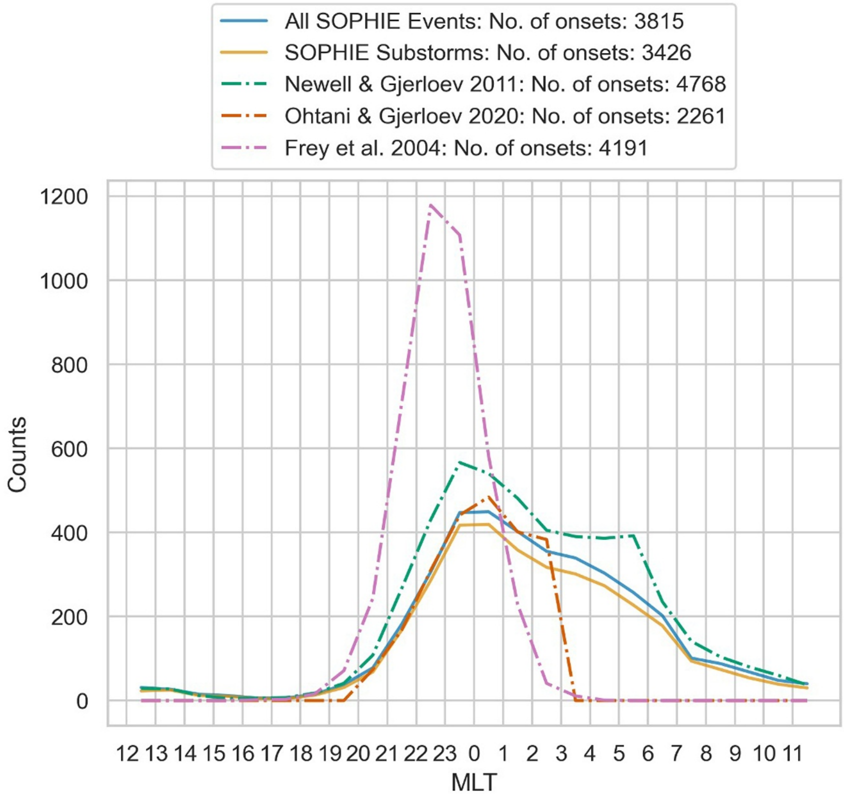

Figure 9. Onset MLT histograms of SOPHIE (All Events in Blue, Substorms in Orange) Newell and Gjerloev (2011) (Green Dashed-Dot), Ohtani and Gjerloev (2020) (Orange Dashed-Dot) and Frey et al. (2004) (Pink Dashed-Dot) events from 19 May 2000 to 31 December 2002. Note that the reduction of events in the Ohtani and Gjerloev (2020) is partly due to the MLT cut-off requirement.

Since it is possible to identify convection enhancements as shown here and in previous work (Shore et al., 2017, 2018) at MLTs where we expect substorms, they cannot simply be filtered out by using the MLT location of the contributing station to SML. Therefore, lists using the SML index alone (Borovsky & Yakymenko, 2017; Newell & Gjerloev, 2011; Ohtani & Gjerloev, 2020) will be populated with false positives, events identified as substorms, but the enhancement in SML is due to convection enhancements or other magnetospheric phenomena. Figure 9 shows the onset MLT distributions from the Frey et al. (2004), Newell and Gjerloev (2011), Ohtani and Gjerloev (2020) and SOPHIE (All events and Only Substorms) from the interval 19 May 2000 and 31 December 2002. In Figure 9, we observe that the MLT distributions of the SML identified events are more similar to each other than to the Frey et al. (2004) MLT distribution. This is in part due to the Frey et al. (2004) events being identified from auroral images, therefore unlikely to be contaminated with DP2 events which do not have the accompanying auroral features that a "true" substorm does. It should also be noted that the MLT distribution of substorm-related Pi2 pulsations (Yeoman et al., 1994) is more similar to that of auroral onsets and our decomposed DP1 distribution, being symmetric and centered on midnight MLT.

As we have shown above that SOPHIE is contaminated with DP2 events and that these can occur within the MLT window of Ohtani and Gjerloev (2020), therefore it is probable that these other onset lists are also contaminated with DP2 events. This issue is one possible source of ambiguity in conducting statistical substorm studies, as the dynamics of other magnetospheric phenomena could be included in with "true" substorms, particularly when relating localized effects throughout the magnetosphere with respect to the substorm. As such, despite considerable progress being made in understanding the characteristic features and consequent effects of the substorm, some conclusions from studies using substorm lists built from magnetic indices may be incomplete because these studies may be considering non-substorm intervals, including other phenomena that are capable of enhancing the electrojets. This ranges from the importance of the phenomenon in the energization and variability of the ring current (Sandhu et al., 2019) and the radiation belts (Forsyth et al., 2016; Rodger, Clilverd, et al., 2022) to its influence on ground-induced currents (Freeman et al., 2019).

One possible route to improve our confidence in identifying substorm intervals could be the use of additional data sets to supplement the auroral indices. One such way of achieving this is by including the behavior of the driver, that is, the solar wind, when identifying substorms. Previous studies have indicated that substorms typically occur after the solar wind has been southward for 22 of the preceding 30 min (Morley & Freeman, 2007). Moreover, the work of Shore et al. (2018) showed that the amplitude of the DP2 pattern is much better correlated with shorter time responses to the IMF than the DP1 pattern. However, taking this approach may have the effect of increasing the number of missed substorm identifications from auroral indices, due to the underlying assumption that substorms cannot occur during strong steady driving.

Another approach integrating other data sets than just the auroral indices was taken by Milan et al. (2021), where they distinguish the AL enhancements due to the substorm from other magnetospheric phenomena by applying the Expanding and Contracting Polar Cap (ECPC) paradigm to event identification. They made use of proxies for the dayside reconnection rate, cross-polar cap potential, as well as the auroral indices to identify the magnetospheric convection state in the year 2010, evaluating between periods of quiet, substorm interval (including the separate phases) and directly driven periods. This approach led to the finding of a lower rate of occurrence of substorms, approximately 550 events per year, than that by Borovsky et al. (1993) or Frey et al. (2004) from injections and auroral intensifications, which identified approximately 1,500 events per year. For reference, during the period analyzed, SOPHIE identified ∼1430 SML enhancement events per year, of which ∼1320 per year were initially identified as substorms; however, our reanalysis showed that only ∼590 of these per year were due to enhancements of the DP1 pattern, similar to the number identified by Milan et al. (2021). In the same period, Newell and Gjerloev (2011) identify ∼1700 substorms per year and Ohtani and Gjerloev (2020) identify ∼950 isolated substorms per year using the SML index, still many more than the proposed number of DP1 events from our reanalysis.

There is also the approach taken by Haiducek et al. (2020) to integrate multiple data sets. In this case they combined multiple already existing substorm lists, based on the AL index, MPB index (Chu et al., 2015), auroral images and particle injections, to more robustly identify events for the month of January 2005. They achieved this by convolving each onset list with Gaussian kernels, that is, they turned an onset time (a unit impulse in time) into a Gaussian onset window centered at the onset time. A substorm onset period was then identified as when a combination of different signatures identified at approximately the same time. This was integrated in the Haiducek et al. (2020) method in a way such that a threshold value was required to be surpassed for a substorm to be identified, but the height of the peak of the Gaussian window from a single signature would not break this threshold. As such, this method requires overlap of multiple detection signatures to indicate a substorm. A full mathematical description of the convolution and combination is available in the full text (Haiducek et al., 2020), where they also evaluate the ability of an MHD model to reproduce the characteristics of substorms. Although a promising pathway for robust identification, a major limitation of this route is the lack of a common description of the substorm by the community or a set of "true" substorms to compare against and tune the parameters for the threshold and kernel width. We also note that the level of co-occurrence of onsets identified from MPB, AL, particle injections and auroral enhancements within 30 min between different substorm signatures is remarkably low, with less than a 50% overlap between pairs of lists based on these identifiers (Lao et al., 2024).

This study highlights some important considerations when conducting studies of substorms. Firstly, it indicates the importance of the separation of AL/SML bays that are due to the substorm and other magnetospheric phenomena. Currently, only SOPHIE (Forsyth et al., 2015) and Milan et al. (2021) attempt to do this by comparing the AL/SML bay with another feature. Ohtani and Gjerloev (2020) makes an attempt at this by limiting identifications to within 23-03 MLT, but our results show there are still a large number of DP2 driven magnetic bays in this local time sector. However, leveraging the SMU index as the SOPHIE technique does is not sufficient to completely isolate the DP1 and DP2 modes of magnetospheric response. Auroral indices are a simplification of a diverse set of observations related to a multitude of processes across multiple scales. This simplification may discard critical data that means that auroral indices do not have enough information to be used to robustly identify substorms. Highlighted above are some possible pathways that could result in a more robust substorm identification schema by including multiple data sets. However, while a promising idea, this is not simple as one must account for the differences in data cadences, coverage, and the time interval covered by the different data sets being used. Moreover, Lao et al. (2024) showed that in the period when there were the auroral indices, mid-latitude indices, auroral imagery, and geosynchronous particle observations available, for a given substorm there is a less than 50% chance that two or more methods will identify it as one. Our study also highlights that caution must be observed when identifying substorms in the dawn sector. Although it is more likely for these events to be DP2 related, it is possible that "true substorms" are detected in this region, highlighting the limitations of a blunt approach such as the one by Ohtani and Gjerloev (2020). When conducting case studies of events identified in this region, we recommend the verification of a true substorm occurrence using another indicator.

Lists of "substorms" are inherently useful in solar terrestrial physics, providing a common baseline for both case and statistical studies of a variety of processes that are part of or result from the phenomena associated with substorms. However, all of these lists have their limitations. Firstly, there is no quantifiable consensus within the solar terrestrial physics community as to what a substorm is, but rather a set of qualitative descriptions of substorm effects, such as the rapid closure of open flux in the magnetotail, brightening and westward expansion of the auroral, injections of energetic particles at geosynchronous orbit, and the formation of magnetic bays at high and mid-latitudes. These effects are not necessarily unique to substorms and may arise from other activity, such as pseudobreakups and steady magnetospheric convection events, and thus may appear in substorm identification lists. SOPHIE attempts to mitigate one of these effects (enhanced magnetospheric convection) and does remove a large number of potential substorms by comparing SML and SMU, but our work shows that this is not perfect. However, we would contend that it provides a better mitigation than limiting identifications to a set of MLT sectors, given the large overlap between the MLT distributions of DP1 and DP2 driven effects. In truth, any list of "substorms" is, in fact, a list of magnetic enhancements, auroral enhancements, particle enhancements, etc. Which may or may not align with substorm activity and should, ultimately, be treated in that way.

5. Summary

In this study, we have used the SOPHIE technique (Forsyth et al., 2015) to quantify the respective contributions of the DP1 and DP2 current patterns to the formation of substorm-like SML bays. This was achieved by evaluating and manipulating the onset MLT, defined as the location of the station that contributes to SML at onset, of various classes of events identified in the SOPHIE phase list. Using the onset MLT distribution of convection enhancements identified by SOPHIE as an indicator of the DP2 event distribution, we were able to decompose a contribution from both DP1 and DP2 to the onset MLT distribution of isolated substorms. We find that although the SOPHIE technique attempts to filter out convection enhancements, 59% of the events originally identified as substorms are instead due to enhancements of the DP2 current pattern, rather than DP1 which is associated with the ionospheric leg of the Substorm Current Wedge. Finally, we explored different values for the threshold used to distinguish between convection enhancements and "true" substorm events and found that no value can distinguish convection events entirely.

We come to the conclusion that the auroral indices, even when filtering events by magnetic local time, are unable to provide sufficient information to robustly identify substorms from enhancements of magnetospheric convection. There is still an invaluable use case for substorm lists using auroral indices in finding events for case studies, which can then be verified as true substorms via other substorm signatures, for example, particle injections, auroral enhancements. However, caution must be exercised when conducting statistical studies related to the substorm phenomena when using these lists as the effects of other magnetospheric modes and phenomena are not entirely removed.

Data Availability Statement

The SMU and SML indices were obtained from the SuperMAG website (https://supermag.jhuapl.edu/). The SOPHIE Forsyth et al. (2015) substorm phase lists used in this study are available in Supporting Information S1 and at the following link: https://doi.org/10.5522/04/28271201.v1. The Frey et al. (2004), Newell and Gjerloev (2011) and Ohtani and Gjerloev (2020) substorm onset lists were accessed from the SuperMAG products webpage (https://supermag.jhuapl.edu/substorms/) and were downloaded on Oct 2021, Feb 2024 and Feb 2024 respectively. The data to reproduce the Shore et al. (2018) polar plots and to create the longitudinal mean profiles were accessed from the Supporting Information S1 of Shore et al. (2018). The code and modified data sets for the analysis and visualization completed in this study are available at Lao (2025).

Acknowledgments

For the SMU and SML indices, we gratefully acknowledge the SuperMAG Collaboration (Gjerloev, 2012): INTERMAGNET, Alan Thomson; CARISMA, PI Ian Mann; CANMOS, Geomagnetism Unit of the Geological Survey of Canada; The S-RAMP Database, PI K. Yumoto and Dr. K. Shiokawa; The SPIDR database; AARI, PI Oleg Troshichev; The MACCS program, PI M. Engebretson; GIMA; MEASURE, UCLA IGPP and Florida Institute of Technology; SAMBA, PI Eftyhia Zesta; 210 Chain, PI K. Yumoto; SAMNET, PI Farideh Honary; IMAGE, PI Liisa Juusola; Finnish Meteorological Institute, PI Liisa Juusola; Sodankylä Geophysical Observatory, PI Tero Raita; UiT the Arctic University of Norway, Tromsø Geophysical Observatory, PI Magnar G. Johnsen; GFZ German Research Centre For Geosciences, PI Jürgen Matzka; Institute of Geophysics, Polish Academy of Sciences, PI Anne Neska and Jan Reda; Polar Geophysical Institute, PI Alexander Yahnin and Yarolav Sakharov; Geological Survey of Sweden, PI Gerhard Schwarz; Swedish Institute of Space Physics, PI Masatoshi Yamauchi; AUTUMN, PI Martin Connors; DTU Space, Thom Edwards and PI Anna Willer; South Pole and McMurdo Magnetometer, PI's Louis J. Lanzarotti and Alan T. Weatherwax; ICESTAR; RAPIDMAG; British Artarctic Survey; McMac, PI Dr. Peter Chi; BGS, PI Dr. Susan Macmillan; Pushkov Institute of Terrestrial Magnetism, Ionosphere and Radio Wave Propagation (IZMIRAN); MFGI, PI B. Heilig; Institute of Geophysics, Polish Academy of Sciences, PI Anne Neska and Jan Reda; University of L'Aquila, PI M. Vellante; BCMT, V. Lesur and A. Chambodut; Data obtained in cooperation with Geoscience Australia, PI Andrew Lewis; AALPIP, co-PIs Bob Clauer and Michael Hartinger; MagStar, PI Jennifer Gannon; LISN PI Cesar Valladares; SuperMAG, PI Jesper W. Gjerloev; Data obtained in cooperation with the Australian Bureau of Meteorology, PI Richard Marshall. CJL was supported by the Science and Technology Facilities Council (STFC) Studentship 2573668. CF was supported by NERC Grants NE/V002724/1 and NE/V002554/2. MPF was supported by NERC Grants NE/V002716/1 and NE/V015133/1. The analysis in this study was performed using Python including the Pandas (Wes McKinney, 2010), NumPy (Harris et al., 2020), Matplotlib (Hunter, 2007), Scikit-learn (Pedregosa et al., 2011) and Seaborn (Waskom, 2021) libraries. The Scientific color map batlow (Crameri, 2023) is used in this study to prevent visual distortion of the data and exclusion of readers with color-vision deficiencies (Crameri et al., 2020).

References

Akasofu, S. I. (1964). The development of the auroral substorm. *Planetary and Space Science*, *12*(4), 273–282. https://doi.org/10.1016/0032-0633(64)90151-5

Akasofu, S. I., Chapman, S., & Meng, C. I. (1965). The polar electrojet. *Journal of Atmospheric and Terrestrial Physics*, *27*(11), 1275–1305. https://doi.org/10.1016/0021-9169(65)90087-5

Amm, O., & Fujii, R. (2008). Separation of Cowling channel and local closure currents in the vicinity of a substorm breakup spiral. *Journal of Geophysical Research*, *113*(A6), A06304. https://doi.org/10.1029/2008JA013021

Borovsky, J. E., Nemzek, R. J., & Belian, R. D. (1993). The occurrence rate of magnetospheric-substorm onsets: Random and periodic substorms. *Journal of Geophysical Research*, *98*(A3), 3807–3813. https://doi.org/10.1029/92JA02556

Borovsky, J. E., & Yakymenko, K. (2017). Substorm occurrence rates, substorm recurrence times, and solar wind structure. *Journal of Geophysical Research: Space Physics*, *122*(3), 2973–2998. https://doi.org/10.1002/2016JA023625

Boström, R. (1964). A model of the auroral electrojets. *Journal of Geophysical Research*, *69*(23), 4983–4999. https://doi.org/10.1029/JZ069i023p04983

Chu, X., McPherron, R. L., Hsu, T.-S., & Angelopoulos, V. (2015). Solar cycle dependence of substorm occurrence and duration: Implications for onset. *Journal of Geophysical Research: Space Physics*, *120*(4), 2808–2818. https://doi.org/10.1002/2015JA021104

Cowling, T. G. (1932). The electrical conductivity of an ionised gas in the presence of a magnetic field. *Monthly Notices of the Royal Astronomical Society*, *93*(1), 90–97. https://doi.org/10.1093/mnras/93.1.90

Coxon, J. C., Freeman, M. P., Jackman, C. M., Forsyth, C., Rae, I. J., & Fear, R. C. (2018). Tailward propagation of magnetic energy density variations with respect to substorm onset times. *Journal of Geophysical Research: Space Physics*, *123*(6), 4741–4754. https://doi.org/10.1029/2017JA025147

Coxon, J. C., Rae, I. J., Forsyth, C., Jackman, C. M., Fear, R. C., & Anderson, B. J. (2017). Birkeland currents during substorms: Statistical evidence for intensification of Regions 1 and 2 currents after onset and a localized signature of auroral dimming. *Journal of Geophysical Research: Space Physics*, *122*(6), 6455–6468. https://doi.org/10.1002/2017JA023967

Crameri, F. (2023). Scientific colour maps. *Zenodo*. https://doi.org/10.5281/zenodo.8409685

Crameri, F., Shephard, G. E., & Heron, P. J. (2020). The misuse of colour in science communication. *Nature Communications*, *11*(1), 1–10. https://doi.org/10.1038/s41467-020-19160-7

Davis, T. N., & Sugiura, M. (1966). Auroral electrojet activity index AE and its universal time variations. *Journal of Geophysical Research*, *71*(3), 785–801. https://doi.org/10.1029/JZ071i003p00785

Dungey, J. W. (1961). Interplanetary magnetic field and the auroral zones. *Physical Review Letters*, *6*(2), 47–48. https://doi.org/10.1103/PhysRevLett.6.47

El-Alaoui, M., Walker, R. J., & McPherron, R. L. (2023). Effects of the ionospheric conductance on the dynamics of the magnetotail. *Journal of Geophysical Research: Space Physics*, *128*(1), e2022JA030259. https://doi.org/10.1029/2022JA030259

Forsyth, C., Rae, I. J., Coxon, J. C., Freeman, M. P., Jackman, C. M., Gjerloev, J., & Fazakerley, A. N. (2015). A new technique for determining substorm onsets and phases from indices of the electrojet (SOPHIE). *Journal of Geophysical Research: Space Physics*, *120*(12), 10592–10606. https://doi.org/10.1002/2015JA021343

Forsyth, C., Rae, I. J., Murphy, K. R., Freeman, M. P., Huang, C.-L., Spence, H. E., et al. (2016). What effect do substorms have on the content of the radiation belts? *Journal of Geophysical Research: Space Physics*, *121*(7), 6292–6306. https://doi.org/10.1002/2016JA022620

Forsyth, C., Sergeev, V. A., Henderson, M. G., Nishimura, Y., & Gallardo-Lacourt, B. (2020). Physical processes of meso-scale, dynamic auroral forms. *Space Science Reviews*, *216*(4), 46. https://doi.org/10.1007/s11214-020-00665-y

Freeman, M. P., Forsyth, C., & Rae, I. J. (2019). The influence of substorms on extreme rates of change of the surface horizontal magnetic field in the United Kingdom. *Space Weather*, *17*(6), 827–844. https://doi.org/10.1029/2018SW002148

Frey, H. U., Mende, S. B., Angelopoulos, V., & Donovan, E. F. (2004). Substorm onset observations by IMAGE-FUV. *Journal of Geophysical Research*, *109*(A10), A10304. https://doi.org/10.1029/2004JA010607

Friis-Christensen, E., Kamide, Y., Richmond, A. D., & Matsushita, S. (1985). Interplanetary magnetic field control of high-latitude electric fields and currents determined from Greenland Magnetometer Data. *Journal of Geophysical Research*, *90*(A2), 1325–1338. https://doi.org/10.1029/JA090iA02p01325

Friis-Christensen, E., & Wilhjelm, J. (1975). Polar cap currents for different directions of the interplanetary magnetic field in the Y-Z plane. *Journal of Geophysical Research*, *80*(10), 1248–1260. https://doi.org/10.1029/JA080i010p01248

Gjerloev, J. W. (2012). The SuperMAG data processing technique. *Journal of Geophysical Research*, *117*(A9), A09213. https://doi.org/10.1029/2012JA017683

Haiducek, J. D., Welling, D. T., Morley, S. K., Ganushkina, N. Y., & Chu, X. (2020). Using multiple signatures to improve accuracy of substorm identification. *Journal of Geophysical Research: Space Physics*, *125*(4), e2019JA027559. https://doi.org/10.1029/2019JA027559

Harris, C. R., Millman, K. J., van der Walt, S. J., Gommers, R., Virtanen, P., Cournapeau, D., et al. (2020). Array programming with NumPy. *Nature*, *585*(7825), 357–362. https://doi.org/10.1038/s41586-020-2649-2

Heppner, J. P. (1954). Time sequences and spatial relations in auroral activity during magnetic bays at College, Alaska. *Journal of Geophysical Research*, *59*(3), 329–338. https://doi.org/10.1029/JZ059i003p00329

Hones, E. W., Jr. (1984). Plasma sheet behavior during substorms. In *Magnetic reconnection in space and laboratory plasmas* (pp. 178–184). American Geophysical Union (AGU). https://doi.org/10.1029/GM030p0178

Hunter, J. D. (2007). Matplotlib: A 2D graphics environment. *Computing in Science & Engineering*, *9*(3), 90–95. https://doi.org/10.1109/MCSE.2007.55

Iijima, T., Potemra, T. A., Zanetti, L. J., & Bythrow, P. F. (1984). Large-scale Birkeland currents in the dayside polar region during strongly northward IMF: A new Birkeland current system. *Journal of Geophysical Research*, *89*(A9), 7441–7452. https://doi.org/10.1029/JA089iA09p07441

Kalmoni, N. M. E., Rae, I. J., Murphy, K. R., Forsyth, C., Watt, C. E. J., & Owen, C. J. (2017). Statistical azimuthal structuring of the substorm onset arc: Implications for the onset mechanism. *Geophysical Research Letters*, *44*(5), 2078–2087. https://doi.org/10.1002/2016GL071826

Kamide, Y., & Kokubun, S. (1996). Two-component auroral electrojet: Importance for substorm studies. *Journal of Geophysical Research*, *101*(A6), 13027–13046. https://doi.org/10.1029/96JA00142

Kepko, L., McPherron, R. L., Amm, O., Apatenkov, S., Baumjohann, W., Birn, J., et al. (2015). Substorm current wedge revisited. *Space Science Reviews*, *190*(1), 1–46. https://doi.org/10.1007/s11214-014-0124-9

Laitinen, J., Holappa, L., & Vanhamäki, H. (2024). The polarity of IMF B strongly modulates particle precipitation during high-speed streams. *Geophysical Research Letters*, *51*(17), e2024GL110877. https://doi.org/10.1029/2024GL110877

Lao, C. J. (2025). Separating DP1 and DP2 current pattern contributions to substorm-like intensifications in SML. *Zenodo*. https://doi.org/10.5281/zenodo.15119811

Lao, C. J., Forsyth, C., Freeman, M. P., Smith, A. W., & Mooney, M. K. (2024). On the association of substorm identification methods. *Journal of Geophysical Research: Space Physics*, *129*(9), e2024JA032762. https://doi.org/10.1029/2024JA032762

Liou, K. (2010). Polar Ultraviolet Imager observation of auroral breakup. *Journal of Geophysical Research*, *115*(A12), A12219. https://doi.org/10.1029/2010JA015578

Lockwood, M. (2023). Universal time effects on substorm growth phases and onsets. *Journal of Geophysical Research: Space Physics*, *128*(11), e2023JA031671. https://doi.org/10.1029/2023JA031671

Maezawa, K. (1976). Magnetospheric convection induced by the positive and negative Z components of the interplanetary magnetic field: Quantitative analysis using polar cap magnetic records. *Journal of Geophysical Research*, *81*(13), 2289–2303. https://doi.org/10.1029/JA081i013p02289

McPherron, R. L. (1970). Growth phase of magnetospheric substorms. *Journal of Geophysical Research*, *75*(28), 5592–5599. https://doi.org/10.1029/JA075i028p05592

McPherron, R. L., & Chu, X. (2017). The mid-latitude positive bay and the MPB index of substorm activity. *Space Science Reviews*, *206*(1), 91–122. https://doi.org/10.1007/s11214-016-0316-6

McPherron, R. L., Russell, C. T., & Aubry, M. P. (1973). Satellite studies of magnetospheric substorms on August 15, 1968: 9. Phenomenological model for substorms. *Journal of Geophysical Research*, *78*(16), 3131–3149. https://doi.org/10.1029/JA078i016p03131

Milan, S. E., Carter, J. A., Sangha, H., Bower, G. E., & Anderson, B. J. (2021). Magnetospheric flux throughput in the Dungey cycle: Identification of convection state during 2010. *Journal of Geophysical Research: Space Physics*, *126*(2), e2020JA028437. https://doi.org/10.1029/2020JA028437

Milan, S. E., Clausen, L. B. N., Coxon, J. C., Carter, J. A., Walach, M.-T., Laundal, K., et al. (2017). Overview of solar wind–magnetosphere–ionosphere–atmosphere coupling and the generation of magnetospheric currents. *Space Science Reviews*, *206*(1), 547–573. https://doi.org/10.1007/s11214-017-0333-0

Morley, S. K., & Freeman, M. P. (2007). On the association between northward turnings of the interplanetary magnetic field and substorm onsets. *Geophysical Research Letters*, *34*(8), L08104. https://doi.org/10.1029/2006GL028891

Newell, P. T., & Gjerloev, J. W. (2011). Evaluation of SuperMAG auroral electrojet indices as indicators of substorms and auroral power. *Journal of Geophysical Research*, *116*(A12), A12211. https://doi.org/10.1029/2011JA016779

Newell, P. T., Meng, C.-I., & Lyons, K. M. (1996). Suppression of discrete aurorae by sunlight. *Nature*, *381*(6585), 766–767. https://doi.org/10.1038/381766a0

Nishida, A., & Kokubun, S. (1971). New polar magnetic disturbances: S, SP, DPC, and DP 2. *Reviews of Geophysics*, *9*(2), 417–425. https://doi.org/10.1029/RG009i002p00417

Nishimura, Y., Lyons, L., Zou, S., Angelopoulos, V., & Mende, S. (2010). Substorm triggering by new plasma intrusion: THEMIS all-sky imager observations. *Journal of Geophysical Research*, *115*(A7), A07222. https://doi.org/10.1029/2009JA015166

Nishimura, Y., Yang, J., Pritchett, P. L., Coroniti, F. V., Donovan, E. F., Lyons, L. R., et al. (2016). Statistical properties of substorm auroral onset beads/rays. *Journal of Geophysical Research: Space Physics*, *121*(9), 8661–8676. https://doi.org/10.1002/2016JA022801

Ohtani, S., & Gjerloev, J. W. (2020). Is the substorm current wedge an ensemble of wedgelets? Revisit to midlatitude positive bays. *Journal of Geophysical Research: Space Physics*, *125*(9), e2020JA027902. https://doi.org/10.1029/2020JA027902

Opgenoorth, H. J., Persson, M. a. L., Pulkkinen, T. I., & Pellinen, R. J. (1994). Recovery phase of magnetospheric substorms and its association with morning-sector aurora. *Journal of Geophysical Research*, *99*(A3), 4115–4129. https://doi.org/10.1029/93JA01502

Østgaard, N., Reistad, J. P., Tenfjord, P., Laundal, K. M., Rexer, T., Haaland, S. E., et al. (2018). The asymmetric geospace as displayed during the geomagnetic storm on 17 August 2001. *Annales Geophysicae*, *36*(6), 1577–1596. https://doi.org/10.5194/angeo-36-1577-2018

Østgaard, N., Stadnes, J., Bjordal, J., Vondrank, R. R., Cummer, S. A., Chenette, D. L., et al. (1999). Global-scale electron precipitation features seen in UV and X rays during substorms. *Journal of Geophysical Research*, *104*(A5), 10191–10204. https://doi.org/10.1029/1999JA900004

Pedregosa, F., Varoquaux, G., Gramfort, A., Michel, V., Thirion, B., Grisel, O., et al. (2011). Scikit-learn: Machine learning in Python. *Journal of Machine Learning Research*, *12*, 2825–2830.

Pulkkinen, T. I., Baker, D. N., Toivanen, P. K., Pellinen, R. J., Friedel, R. H. W., & Korth, A. (1994). Magnetospheric field and current distributions during the substorm recovery phase. *Journal of Geophysical Research*, *99*(A6), 10955–10966. https://doi.org/10.1029/93JA02718

Rae, I. J., Watt, C. E. J., Murphy, K. R., Frey, H. U., Ozeke, L. G., Milling, D. K., & Mann, I. R. (2012). The correlation of ULF waves and auroral intensity before, during and after substorm expansion phase onset. *Journal of Geophysical Research*, *117*(A8), A08213. https://doi.org/10.1029/2012JA017534

Rodger, C. J., Clilverd, M. A., Hendry, A. T., & Forsyth, C. (2022a). Examination of radiation belt dynamics during substorm clusters: Magnetic local time variation and intensity of precipitating fluxes. *Journal of Geophysical Research: Space Physics*, *127*(12), e2022JA030750. https://doi.org/10.1029/2022JA030750

Rodger, C. J., Hendry, A. T., Clilverd, M. A., Forsyth, C., & Morley, S. K. (2022b). Examination of radiation belt dynamics during substorm clusters: Activity drivers and dependencies of trapped flux enhancements. *Journal of Geophysical Research: Space Physics*, *127*(1), e2021JA030003. https://doi.org/10.1029/2021JA030003

Sandhu, J. K., Rae, I. J., Freeman, M. P., Gkioulidou, M., Forsyth, C., Reeves, G. D., et al. (2019). Substorm-ring current coupling: A comparison of isolated and compound substorms. *Journal of Geophysical Research: Space Physics*, *124*(8), 6776–6791. https://doi.org/10.1029/2019JA026766

Shore, R. M., Freeman, M. P., & Gjerloev, J. W. (2018). An empirical orthogonal function reanalysis of the northern polar external and induced magnetic field during solar cycle 23. *Journal of Geophysical Research: Space Physics*, *123*(1), 781–795. https://doi.org/10.1002/2017JA024420

Shore, R. M., Freeman, M. P., Wild, J. A., & Gjerloev, J. W. (2017). A high-resolution model of the external and induced magnetic field at the Earth's surface in the Northern Hemisphere. *Journal of Geophysical Research: Space Physics*, *122*(2), 2440–2454. https://doi.org/10.1002/2016JA023682

Smith, A. W., Rae, I. J., Forsyth, C., Coxon, J. C., Walach, M.-T., Lao, C. J., et al. (2024). Space weather forecasts of ground level space weather in the UK: Evaluating performance and limitations. *Space Weather*, *22*(11), e2024SW003973. https://doi.org/10.1029/2024SW003973

Smith, A. W., Rae, I. J., Forsyth, C., Watt, C. E. J., & Murphy, K. R. (2020). On the magnetospheric ULF Wave counterpart of substorm onset. *Journal of Geophysical Research: Space Physics*, *125*(4), e2019JA027573. https://doi.org/10.1029/2019JA027573

Tanskanen, E., Pulkkinen, T. I., Koskinen, H. E. J., & Slavin, J. A. (2002). Substorm energy budget during low and high solar activity: 1997 and 1999 compared. *Journal of Geophysical Research*, *107*(A6). https://doi.org/10.1029/2001JA900153

Walker, S. J., Laundal, K. M., Reistad, J. P., Hatch, S. M., Ohma, A., & Gjerloev, J. (2024). The ionospheric leg of the substorm current wedge: Combining iridium and ground magnetometers. *Journal of Geophysical Research: Space Physics*, *129*(7), e2024JA032414. https://doi.org/10.1029/2024JA032414

Wallis, D. D., & Budzinski, E. E. (1981). Empirical models of height integrated conductivities. *Journal of Geophysical Research*, *86*(A1), 125–137. https://doi.org/10.1029/JA086iA01p00125

Wang, H., Lühr, H., Ma, S. Y., & Ritter, P. (2005). Statistical study of the substorm onset: Its dependence on solar wind parameters and solar illumination. *Annales Geophysicae*, *23*(6), 2069–2079. https://doi.org/10.5194/angeo-23-2069-2005

Waskom, M. L. (2021). Seaborn: Statistical data visualization. *Journal of Open Source Software*, *6*(60), 3021. https://doi.org/10.21105/joss.03021

Waters, J. E., Jackman, C. M., Whiter, D. K., Forsyth, C., Fogg, A. R., Lamy, L., et al. (2022). A perspective on substorm dynamics using 10 years of auroral kilometric radiation observations from wind. *Journal of Geophysical Research: Space Physics*, *127*(9), e2022JA030449. https://doi.org/10.1029/2022JA030449

Weimer, D. R. (1994). Substorm time constants. *Journal of Geophysical Research*, *99*(A6), 11005–11015. https://doi.org/10.1029/93JA02721

Wes McKinney. (2010). Data structures for statistical computing in Python. In S. van der Walt, & J. Millman (Eds.), *Proceedings of the 9th Python in science conference* (pp. 56–61). https://doi.org/10.25080/Majora-92bf1922-00a

Yeoman, T. K., Freeman, M. P., Reeves, G. D., Lester, M., & Orr, D. (1994). A comparison of midlatitude Pi 2 pulsations and geostationary orbit particle injections as substorm indicators. *Journal of Geophysical Research*, *99*(A3), 4085–4093. https://doi.org/10.1029/93JA03233